Electronic Supplementary Information

DFT computations combined with semiempirical modeling of variations with temperature of spectroscopic and magnetic properties of Gd^{3+}-doped $PbTiO_3$

Muhammed Acikgoz[1], Leila Mollabashi[2], Shahrbano Rahimi[2], Saeid Jalali-Asadabadi[2], Czesław Rudowicz[3]
[1] *Department of Science, The State University of New York (SUNY) Maritime College, New York 10465, USA.*
[2]*Department of Physics, Faculty of Physics, University of Isfahan (UI), Hezar Jerib Avenue, Isfahan 81746-73441, Iran*
[3]*Faculty of Chemistry, A. Mickiewicz University (AMU), 61-614 Poznań, Poland*

TABLE OF CONTENTS

I. SPM expressions for ZFS parameters

II. Atomic multiplicity, equivalence, and nonequivalence of the unit cell and supercells

III. Computational Details

III.1. Temperature-dependent DFT computations

III.2. Methods utilized for optimization of structural properties

III.3. Relativistic aspects in the calculations of the formation energies

III.4. Procedure used for determination of stoichiometry of the doped compositions

Tables and Figures

I. SPM expressions for ZFS parameters

The general explicit SPM/ZFSP expressions given below are suitable for Gd^{3+} (S = 7/2) ion coordinated by *n*-ligands in the metal-ligand ML_n complex exhibiting tetragonal site symmetry. For Gd^{3+}:$PbTiO_3$ the coordination number $n = 6$ for Ti site and 12 for Pb site. In Eqs. (S1) – (S3) the symbols have the following meaning: (R_i, θ_i, φ_i) are the polar coordinates of the *i*-th ligand, the intrinsic parameters $\bar{b}_k(R_0)$ represent the strength of the k^{th}-rank ZFS contributions from a given ligand type located at the distance R_i, R_0 is the reference distance, which in practice is arbitrarily fixed as the average M-L distance R_{avg} for a particular ML_n complex, t_k are the power-law exponents.[1,2,3]

$$b_2^0 = \frac{\bar{b}_2(R_0)}{2}\left[\left(\frac{R_0}{R_i}\right)^{t_2}\sum_{i=1}^{n}\left(3\cos^2\theta_i - 1\right)\right]. \qquad \text{(S1)}$$

$$b_4^0 = \frac{\bar{b}_4(R_0)}{8}\left[\left(\frac{R_0}{R_i}\right)^{t_4}\sum_{i=1}^{n}\left(35\cos^4\theta_i - 30\cos^2\theta_i + 3\right)\right]$$
$$b_4^4 = \frac{35}{8}\bar{b}_4(R_0)\left[\left(\frac{R_0}{R_i}\right)^{t_4}\sum_{i=1}^{n}\sin^4\theta_i\cos 4\varphi_i\right] \quad \text{(S2)}$$
$$b_6^0 = \frac{\bar{b}_4(R_0)}{16}\left[\left(\frac{R_0}{R_i}\right)^{t_6}\sum_{i=1}^{n}\left(231\cos^6\theta_i - 315\cos^4\theta_i + 105\cos^2\theta_i - 5\right)\right]$$
$$b_6^4 = \frac{63}{16}\bar{b}_4(R_0)\left[\left(\frac{R_0}{R_i}\right)^{t_6}\sum_{i=1}^{n}\sin^4\theta_i(11\cos^2\theta_i - 1)\cos 4\varphi_i\right] \quad . \quad \text{(S3)}$$
$$b_6^6 = \frac{231}{32}\bar{b}_4(R_0)\left[\left(\frac{R_0}{R_i}\right)^{t_6}\sum_{i=1}^{n}\sin^6\theta_i\cos 6\varphi_i\right]$$

II. Atomic multiplicity, equivalence, and nonequivalence of the unit cell and supercells

The unit cell of the pure $PbTiO_3$ compound constitutes of one Pb, one Ti, and three O atoms, where only two of the three oxygen atoms are non-equivalent. The multiplicity of the first kind of oxygen (O1) is one, while the multiplicity of the second kind of oxygen atom (O2) is two. This implies that there are one O1 and two equivalent O2 atoms in the unit cell. The unit cell contains $5(=1+1+3)$ atoms, including $4(=1+1+2)$ non-equivalent atoms. In summary, in the unit cell, there are five atoms, i.e., 1×Pb, 1×Ti, 2×O1, 1×O2, and four non-equivalent atoms, i.e., Pb, Ti, O1, O2, *viz.*, $(5)_{\text{atoms}} = (1)_{\text{Pb}} + (1)_{\text{Ti}} + (2+1)_{\text{O}}$ and $(4)_{\text{non-equivalent atoms}} = (1)_{\text{Pb}} + (1)_{\text{Ti}} + (1+1)_{\text{O}}$. The $2\times2\times2$ supercell contains 8 Pb including 6 non-equivalent Pb atoms, 8 Ti including 2 non-equivalent Ti atoms, and 24 O including 6 non-equivalent O atoms. The multiplicity factor is 2 for 2 of the 6 Pb atoms, while this factor is 1 for the remaining 4 Pb atoms, *viz.*, $8(=2\times2+1\times4)$. The multiplicity factor is 4 for both of the Ti atoms, *viz.*, $8(=4\times2)$. The multiplicity factor is 4 for the 6 O atoms, *viz.*, $24(=4\times6)$. In summary, the supercell contains $40(=8+8+24)$ atoms, including $14(=6+2+6)$ non-equivalent atoms. In summary, in the supercell there are forty atoms, i.e., 1×Pb1, 2×Pb2, 1×Pb3, 1×Pb4, 2×Pb5, 1×Pb6, 4×Ti1, 4×Ti2, 4×O1, 4×O2, 4×O3, 4×O4, 4×O5, 4×O6, and fourteen non-equivalent atoms, i.e., Pb1, Pb2, Pb3, Pb4, Pb5, Pb6, Ti1, Ti2, O1, O2, O3, O4, O5, O6, *viz.*, $(40)_{\text{atoms}} = (1+2+1+1+2+1)_{\text{Pb}} + (4+4)_{\text{Ti}} + (4+4+4+4+4+4)_{\text{O}}$ and $(14)_{\text{non-equivalent atoms}} = (1+1+1+1+1+1)_{\text{Pb}} + (1+1)_{\text{Ti}} + (1+1+1+1+1+1)_{\text{O}}$. The same supercell, as discussed above, is used to substitute Gd atom at Pb-site. However, to construct $PbTi_{0.0875}Gd_{0.125}O_3$, we have used another $2\times2\times2$ supercell. This new supercell contains 8 Pb, including 2 non-equivalent Pb atoms, 1 Gd atom, 7 Ti, including 5 non-equivalent Ti atoms, and 24 O, including 10 non-equivalent

O atoms. The multiplicity factor is 4 for both of the Pb atoms, *viz.*, $8(=4\times2)$. The multiplicity factors are 1, 2, and 4, for 4, 2, and 4 for 4 of the 10 O atoms, *viz.*, $24(=1\times4+2\times2+4\times4)$. In summary, the supercell contains $40(=8+1+7+24)$ atoms, including $18(=2+1+5+10)$ non-equivalent atoms. Moreover, for $PbTi_{0.875}Gd_{0.125}O_{3-\delta}$ the similar $2\times2\times2$ supercell with one less O atom is used, *viz.*, 23 O including 9 non-equivalent O atoms.

In order to investigate the O vacancy defect in $Pb_{0.875}Gd_{0.125}TiO_{3-\delta}$, we have used a $2\times2\times2$ supercell, containing 7 Pb including 5 non-equivalent Pb atoms, 1 Gd atoms, 8 Ti, including 6 non-equivalent Ti atoms, and 23 O, including 13 non-equivalent O atoms. The multiplicity factor is 2 for 2 of the Pb atoms and 1 for the 3 remaining Pb atoms, *viz.*, $7(=2\times2+1\times3)$. For 2 of Ti atoms the multiplicity factor is 2 and 1 for the others, *viz.*, $8(=2\times2+1\times4)$. As well, the multiplicity factor of 10 O atoms is 2 and the 3 others O is 1, *viz.*, $23(=2\times10+1\times3)$.

III. Computational Details

III.1. Temperature-dependent DFT computations

The two procedures that allow to include higher temperatures in DFT computations are as follows.

(1) One procedure is to multiply the density of states (DOS) by the Fermi-Dirac distribution. Here we assume that the temperature is not so high to change the shape of the ground state band structure and only the arrangements of electrons are changed by the increasing temperature according to the Pauli exclusion principle. It is worth mentioning that although in this procedure ion dynamics is ignored before performing DFT computations, temperature dependence can be still included after obtaining electronic band structures at zero temperature. In order to elucidate the latter point, we discuss the effects of multiplying the DOS, i.e., $g(\varepsilon)$, by the Fermi-Dirac distribution function, $f(\varepsilon)$. At zero temperature ($T=0$), where the chemical potential μ approaches to the Fermi energy ε_F, as expressed in Eq. (2.53) of Ref.[4], $f(\varepsilon)$ becomes a step function, as written in Eq. (2.52) of Ref. [4], that is unity before ε_F and zero after ε_F. Therefore, at $T=0$, this step function implies that all the valence states under the Fermi energy are occupied, while all the conduction states above the Fermi level remain unoccupied, as shown in Fig. 2.3(a) of Ref.[4] However, at $T\neq0$, $f(\varepsilon)$, as expressed in Eq. (2.56) of Ref. [4], deviates from the step function so that some of the electrons are allowed to move from the valence states towards the conduction states depending on how much the temperature has increased from zero, as shown in Fig. 2.3(b) of Ref. [4] Therefore, multiplying the $g(\varepsilon)$ by $f(\varepsilon)$ at $T\neq0$ allows to consider temperature dependence of the physical quantities. For example, at $T\neq0$ the energy density, $u=U/V$, and electron density, $n=N/V$, can be obtained as $u=\int_{-\infty}^{\infty}\varepsilon g(\varepsilon)f(\varepsilon)d\varepsilon$ and $n=\int_{-\infty}^{\infty}g(\varepsilon)f(\varepsilon)d\varepsilon$, as expressed in Eqs. (2.66) and (2.67) of Ref. [4], respectively. In the integrands of the latter integrals, $g(\varepsilon)$ is multiplied by $f(\varepsilon)$ to consider the effects of temperature on the energy and electron densities,

respectively. For the other physical quantities, depending on how they are related to total energy, the derivatives of the Fermi-Dirac distribution functions may appear in the integrands, see e.g., electronic specific heat capacity expressed in Eq. (28) on page 152 of Ref.[5] as $C_{el} = \frac{dU}{dT} = \int_0^\infty d\varepsilon(\varepsilon - \varepsilon_F)\frac{df(\varepsilon)}{dT}g(\varepsilon)$. In the latter integral, temperature dependency of C_{el} is considered within the temperature derivative of the $f(\varepsilon)$. We have recently also used the same strategy to study the thermoelectric properties of cerium-based compounds, where the temperature dependences of Seebeck coefficient and electrical conductivity have been used within the energy derivative of $f(\varepsilon)$, as expressed in Eqs. (3) and (4) of Ref. [6], respectively, as well as the electronic part of the thermal conductivity expressed in Eq. (3) Ref. [7]. The above discussion confirms that using the procedure (1) ion dynamics is not directly included before performing the electronic structure computations. Therefore, it represents a purely electronic approach where phonon vibrations have been neglected.

In this purely electronic approach, the band structure is obtained at zero temperature in the absence of ion dynamics and then the effects of a nonzero temperature are considered using the Fermi-Dirac distribution function at a specific temperature. By this way, the electronic part of the temperature dependence of a physical quantity can be estimated for a given crystal. In order to consider the phononic part of the temperature dependence of a physical quantity, ion dynamics would be also included. In this work, we have included neither electronic nor ionic temperature dependence in DFT computations. Hence, our ground state results are obtained at zero temperature.

(2) Using temperature dependent density functional theory where temperature can be considered by going beyond the standard Kohn-Sham DFT formalism via time dependent DFT (TDDFT). The TDDFT, as an extension of the standard Kohn-Sham DFT, is a quantum mechanical theory utilized to study the dynamics of the many-body systems in question involving time-dependent potentials. Here, we have used time or temperature independent DFT. Note that we have used the cif files measured at nonzero temperatures. Hence, in fact, we have calculated the ground state electronic structures of the systems observed at nonzero temperatures. Ground state here again implies that the electronic structures are calculated by DFT at zero temperature. For considering higher temperature, we would redistribute the electrons following the Pauli exclusion principle and find the excited states of system where some valence electrons can move to the conduction region. Here, we have not done it and so our results are related to the ground state of the system. Note that the temperature is considered, albeit indirectly, via the structures measured at nonzero temperature without applying Fermi-Dirac distribution function or employing time/high-temperature dependent DFT.

III.2. Methods utilized for optimization of structures, structural properties, and electronic structures

For the optimization of structures, and computation of structural properties, we use the semilocal PBE-GGA functional.[11] Structural properties, such as lattice constants, bulk moduli, and elastic constants, can be usually well predicted consistent with experiment more quickly by the local and semilocal functionals, such as LDA and PBE-GGA, than the other more sophisticated and time-consuming functionals, such as hybrid, LDA+U, GW, with more

expensive costs of calculations. [12] However, it is well-known that the (LDA) and PBE-GGA cannot always satisfactorily predict the electronic structures of the strongly correlated systems due to its weakness in predicting the degree of 4f electrons localization. [8,9] This shortcoming of LDA and PBE-GGA originates from the dual nature of the 4f and/or 5f electrons.[10] The nature of the 4f electrons varies between two extreme limits, i.e., itinerant and localized behaviors.[6] Therefore, to go beyond the PBE-GGA functional including onsite-exact-exchange, i.e., Hartree-Fock (HF), we use the hybrid functional[11] to consider the strong electronic correlations of the 4f electrons in Gd^{3+} ions. Generally, hybrid functional can be written as: $E_{xc}^{hybrid} = E_{xc}^{SL} + \alpha(E_x^{HF} - E_x^{SL})$, where some parts of the exchange term in the semilocal functional is replaced by the HF exchange. In this expression, α is a dimensionless mixing parameter describing the fraction of the HF exchange. The E_{xc} and E_x are the exchange-correlation and exchange functionals, respectively. Nominally, α can vary between: 0 and 1, *viz.* $0 \leq \alpha \leq 1$. For $\alpha = 0$, the hybrid functional E_{xc}^{hybrid}reduces to the semilocal functional E_{xs}^{SL}, *viz.* $E_{xc}^{hybrid} = E_{xs}^{SL} + 0 \times (E_x^{HF} - E_x^{SL}) = E_{xs}^{SL}$. Thus, the lower limit, $\alpha = 0$, refers to the PBE-GGA functional with lower degree of 4f-localization. For $\alpha = 1$, the hybrid functional E_{xc}^{hybrid}simplifies to the onsite-exact-exchange functional E_x^{HF}, *viz.* $E_{xc}^{hybrid} = E_{xs}^{SL} + 1 \times (E_x^{HF} - E_x^{SL}) = E_{xs}^{SL} + E_x^{HF} - E_x^{SL} = E_x^{HF}$. Thus, the upper limit, $\alpha = 1$, represents the HF exchange functional with higher degree of 4f-localization. In practice, the α parameter can be fine-tuned by matching to experimental data, if available. For the pure compound, the semilocal PBE-GGA functional yields appropriate results. This implies that for the pure compound, it is not essential to include more correlations, since there are no 4f correlated electrons.

In this work, the correlated orbital is the localized 4f orbital of Gd ion which exists only after doping Gd. To increase the accuracy of the calculations, we use the hybrid functional only for the electronic properties of the doped compounds containing Gd^{3+} ions. The reason is that the computed structural properties are less sensitive to the correlation effects than the computed electronic properties. This finding is corroborated by comparing Table 1 and Table 2 of Ref.[12] reporting the lattice parameters and Bulk moduli (i.e., structural properties), and the magnetic moments (i.e., electronic structures), respectively, for $CeIn_3$ heavy fermion system. This comparison shows that the lattice parameters and Bulk moduli computed by semilocal functional agree well with experimental values, whereas much worse agreement is observed for the magnetic moments computed by semilocal functional and experimental values. By including hybrid functional over semilocal functional, the electronic properties that are highly sensitive to the correlation effects may be perceptibly improved, whereas no such gain can be obtain for structural properties, see Tables 1 and 2 of Ref. [12]

Therefore, for the doped compounds, we use the hybrid (PBE-GGA) functional as the semilocal exchange-correlation functional to calculate their electronic (structural) properties that are highly (slightly) sensitive to the correlation effects. However, due to the lack of experimental data for the doped compounds, it is impossible to adjust the mixing parameter α by matching the computed and experimental data. Nevertheless, in practice, the

variation range of this parameter is smaller than that nominally expected (0, 1). According to the available experiences, the values of α ranging from 0.2 to 0.3 usually yields appropriate results, see Table 1 and Fig. 1 of Ref. [12] Note that the default value of α = 0.25, optimized by taking a variety of strongly correlated compounds into account, is adopted in the WIEN2k code; for details, see, in Ref. [13] Section 4.5.8 "Onsite-exact-exchange and hybrid functionals for correlated electrons", formula expressed on page 50, and the corresponding value of α parameter given in the last line of the "case.ineece" file on page 51, where the extension "ineece" stands for input (IN) for the exact exchange for correlated electrons (EECE). [14] Importantly, e.g. Bjaalie et al. [15] obtained satisfactory results using $\alpha = 0.25$ for $GdTiO_3$ crystal, which is structurally similar to Gd^{3+}:$PbTiO_3$ studied by us. Hence, we also adopt of α = 0.25 for the hybrid calculations.

III.3. Relativistic interactions included in the DFT computations and its effects on the physical results

The relativistic corrections can affect the DFT band structures and thus physical properties, when the velocity of electron approaches to that of light. Taking the relativistic interaction into account makes the *ab initio* calculations more cumbersome and computationally expensive. The relativistic effects depend on the atomic numbers of the atoms that make up the compounds as well as the crystalline environment of the material. In free atoms, the relativistic effects can become more crucial for heavy atoms having high atomic numbers.[16] In compounds containing heavy atoms, in addition to the atomic numbers, the relativistic effects can also depend on the interactions occurring within the crystals, as determined by the electronic structures of the materials. For instance, we have previously concluded that the relativistic effects may not be so significant for Pb/Si(111) thin-films, despite containing heavy Pb atom.[17] However, we would not generalize the latter conclusion to the cases in question due to the following reasons: (1) in addition to the Pb atom, the doped cases contain heavy Gd atoms with large atomic number 64, (2) the crystalline environments of the pure and doped compounds differ from that of Pb/Si(111) thin-films, and (3) in principle, including the relativistic effect can generally provide more accurate results than in the case they are excluded. Therefore, despite making the calculations more time-consuming, we have considered the relativistic effects for the pure compound, including the heavy Pb atom, and the doped compositions, including both the Pb and Gd atoms. In one of the initialization steps using the WIEN2k code, before performing self-consistent field (SCF) calculations, we separate the electrons into core and valence electrons by giving a separation energy of -9.0 Ry. In this step, the core electrons are solved by LSTRART program, which is a modified multiconfiguration relativistic Dirac-Fock program.[18] For the valence electrons, the fully relativistic Dirac equation, as expressed in Eq. (1) of Ref. X =[http://wien2k.at/reg_user/textbooks/novak_lecture_on_spinorbit.pdf}], is simplified to Eq. (10) in Ref. X. Using central filed approximation, i.e., assuming spherical symmetry, the above simplified Dirac equation is further reduced to Eq. (11) in Ref. X, which includes five terms. In so-reduced equation, the first and second terms are the common nonrelativistic Schrödinger equation, the third term is the mass correction, the fourth term is

the Darwin correction, and the fifth term represents the spin-orbit coupling (SOC). In this work, the SOC is added to include the relativistic effects using the second variational method.[19]

III.4. Procedure used for determination of stoichiometry of the doped compositions

To consider the stoichiometry of the doped compositions in the absence and presence of the oxygen vacancy, we adopt the following three-step procedure (briefly outlined in Section 4.4 of the Main part). In the first step, we construct a $2 \times 2 \times 2$ supercell so that the 1:1:3 stoichiometry of the pure compound remains unchanged. The $2 \times 2 \times 2$ supercell contains eight $PbTiO_3$ formula units and is denoted $Pb_8Ti_8O_{24}$. The stoichiometry of the pure $Pb_8Ti_8O_{24}$ is 8:8:24. The latter stoichiometry of the pure compound inside the supercell can be simplified after dividing by 8 to $\left(\frac{8}{8}:\frac{8}{8}:\frac{24}{8}\right)$, which is identical to the stoichiometry $(1:1:3)$ of the pure $PbTiO_3$ inside the unit cell. This structural model ensures that the charges are still compensated in $Pb_8Ti_8O_{24}$, *viz.*, $8 \times (+2e) + 8 \times (+4e) + 24 \times (-2e) = 16e + 32e - 48e = 0$.

In the second step, we doped Gd at the Pb (Ti) site, leading to $Pb_7GdTi_8O_{24}$ ($Pb_8Ti_7GdO_{24}$) with the stoichiometry of $7:1:8:24$ $(8:7:1:24)$. The latter stoichiometry of the doped compound inside the supercell can be simplified, after dividing by 8, to $\frac{7}{8}:\frac{1}{8}:\frac{8}{8}:\frac{24}{8}$ $\left(\frac{8}{8}:\frac{7}{8}:\frac{1}{8}:\frac{24}{8}\right)$, which is identical to $0.875:0.125:1:3$ $(1:0.875:0.125:3)$, corresponding to the doped compound $Pb_{0.875}Gd_{0.125}TiO_3$ ($PbTi_{0.875}Gd_{0.125}O_3$). In this model, the charges are not compensated in $Pb_{0.875}Gd_{0.125}TiO_3$ ($PbTi_{0.875}Gd_{0.125}O_3$) leading to extra $+0.125e$ $(-0.125e)$ charges, *viz.*, $\frac{7}{8} \times (+2e) + \frac{1}{8} \times (+3e) + 1 \times (+4e) + 3 \times (-2e) = \frac{17}{8}e + 4e - 6e = \frac{17}{8}e + \frac{32}{8}e - \frac{48}{8}e = \frac{1}{8}e = +0.125e$ $\left(1 \times (+2e) + \frac{7}{8} \times (+4e) + \frac{1}{8} \times (+3e) + 3 \times (-2e) + 3 \times (-2e) = 2e + \frac{28}{8}e + \frac{3}{8}e - 6e = \frac{16}{8}e + \frac{28}{8}e + \frac{3}{8}e - \frac{48}{8}e = -\frac{1}{8}e = -0.125e\right)$. This shows that the charges are not balanced for doped compositions in the absence of the oxygen vacancy. However, in our DFT/*ab initio* computations, the valences (electron charges) are determined so that in any case the system remains neutral and the charges are well balanced due to the hybridizations occurring among various orbitals of the atoms in both the doped compositions in the absence of the oxygen vacancy.

In the third step, we introduce an oxygen vacancy (denoted customarily[20] by an empty square symbol □) at the O site, which leads to $Pb_7GdTi_8O_{23}\square_1$ ($Pb_8Ti_7GdO_{23}\square_1$) with the stoichiometry of $7:1:8:23:1$ $(8:7:1:23:1)$. The latter stoichiometry of the doped compound in the presence of oxygen vacancy inside the supercell can be simplified after dividing by 8 to $\frac{7}{8}:\frac{1}{8}:\frac{8}{8}:\frac{23}{8}:\frac{1}{8}$ $\left(\frac{8}{8}:\frac{7}{8}:\frac{1}{8}:\frac{23}{8}:\frac{1}{8}\right)$, which is identical to $0.875:0.125:1:2.875:1.125$ $(1:0.875:0.125:2.875:1.125)$, corresponding to the doped compound $Pb_{0.875}Gd_{0.125}TiO_{2.875}\square_{0.125}$ ($PbTi_{0.875}Gd_{0.125}O_{2.875}\square_{0.125}$). By the above assumption, the charges are not compensated in $Pb_{0.875}Gd_{0.125}TiO_{2.875}\square_{0.125}$ ($PbTi_{0.875}Gd_{0.125}O_{2.875}\square_{0.125}$) leading to extra $+0.375e$ $(+0.125e)$ charges, *viz.*,

$\frac{7}{8}\times(+2e)+\frac{1}{8}\times(+3e)+\frac{8}{8}\times(+4e)+\frac{23}{8}\times(-2e)+\frac{1}{8}\times(0e)=\frac{14}{8}e+\frac{3}{8}e+\frac{32}{8}e-\frac{46}{8}e=\frac{3}{8}e=+0.375e$ $\left(\frac{8}{8}\times(+2e)+\frac{7}{8}\times(+4e)+\frac{1}{8}\times(+3e)+\frac{23}{8}\times(-2e)+\frac{1}{8}\times(0e)=\frac{16}{8}e+\frac{28}{8}e+\frac{3}{8}e-\frac{46}{8}e=\frac{16}{8}e+\frac{28}{8}e+\frac{3}{8}e-\frac{46}{8}e=+\frac{1}{8}e=+0.125e\right)$. For convenience, in the Main part the latter doped compound in the presence of the oxygen vacancy is represented as $Pb_{0.875}Gd_{0.125}TiO_{3-\delta}$ ($PbTi_{0.875}Gd_{0.125}O_{3-\delta}$), i.e. with the symbol □ replaced for short by the symbol δ; here, $\delta = 0.125 = \frac{1}{8}$. Using this notation, the stoichiometry of the latter doped compound in the presence of oxygen vacancy can be simplified as: $\frac{7}{8}:\frac{1}{8}:\frac{8}{8}:\frac{23}{8}$ $\left(\frac{8}{8}:\frac{7}{8}:\frac{1}{8}:\frac{23}{8}\right)$, i.e. $0.875:0.125:1:2.875$ $(1:0.875:0.125:2.875)$ for $Pb_{0.875}Gd_{0.125}TiO_{3-\delta}$ ($PbTi_{0.875}Gd_{0.125}O_{3-\delta}$), respectively. This leads to the same extra charges:$+0.375e$ $(+0.125e)$, *viz.*, $\frac{7}{8}\times(+2e)+\frac{1}{8}\times(+3e)+1\times(+4e)+\frac{23}{8}\times(-2e)=\frac{14}{8}e+\frac{3}{8}e+\frac{32}{8}e-\frac{46}{8}e=\frac{3}{8}e=+0.375e$ $\left(1\times(+2e)+\frac{7}{8}\times(+4e)+\frac{1}{8}\times(+3e)+\frac{23}{8}\times(-2e)=\frac{16}{8}e+\frac{28}{8}e+\frac{3}{8}e-\frac{46}{8}e=\frac{16}{8}e+\frac{28}{8}e+\frac{3}{8}e-\frac{46}{8}e=+\frac{1}{8}e=+0.125e\right)$.

Tables and Figures

Table S1. The ligand bond lengths (in [Å]) and the angular positions (in [°]) of O^{2-} ligands in the $[Ti\text{-}O_6]^{8-}$ cluster for the Gd^{3+} center in $PbTi_{0.875}Gd_{0.125}O_3$: (a) non-relaxed structure obtained from the cif file[21] and (b) optimized relaxed structure after DFT optimization.

	(a) Non-relaxed			(b) Relaxed Ti1 site			(b) Relaxed Ti2 site			(b) Relaxed Gd site		
Ligand	R_{i0}	θ_i	φ_i	R_{i0}	θ_i	φ_i	R_{i0}	θ_i	φ_i	R_{i0}	θ_i	φ_i
O1	2.3719	0	0	2.4793	0	0	2.5229	0	0	2.3225	0	0
O1	1.7628	180	0	1.7760	180	0	1.7653	180	0	2.1070	180	0
O2	1.9698	81.47	0	1.9089	76.20	0	2.0007	78.81	0	2.1446	81.76	0
O2	1.9698	81.47	90	2.0447	80.27	90	2.0007	78.81	90	2.1446	81.76	90
O2	1.9698	81.47	180	1.9089	76.20	180	2.0007	78.81	180	2.1446	81.76	180
O2	1.9698	81.47	270	2.0447	80.27	270	2.0007	78.81	270	2.1446	81.76	270

Table S2. The ligand bond lengths (in [Å]) and the angular positions (in [°]) of O^{2-} ligands in the $[Pb\text{-}O_{12}]^{22-}$ cluster for the Gd^{3+} center in $Pb_{0.875}Gd_{0.125}TiO_3$: (a) non-relaxed structure obtained from the cif file[21] and (b) optimized relaxed structure after DFT optimization for the Pb substitution sites of type: (1) {Pb1, Pb5, Pb2, or Pb6} and type (2) {Pb3, Pb7, Pb4, or Pb8}.

	(a) Non-relaxed Pb site			(b) Relaxed Pb type (1) site			(b) Relaxed Pb type (2) site			(b) Relaxed Gd site		
Ligand	R_{i0}	θ_i	φ_i	R_{i0}	θ_i	φ_i	R_{i0}	θ_i	φ_i	R_{i0}	θ_i	φ_i
O1	2.7917	80.691	45	2.8213	80.538	45	3.0494	80.684	45	2.5990	76.856	45
O1	2.7917	80.691	135	2.8213	80.538	135	3.0494	80.684	135	2.5991	76.856	135
O1	2.7917	80.691	225	2.8213	80.538	225	3.0494	80.684	225	2.5991	76.856	225
O1	2.7917	80.691	315	2.8213	80.538	319.87	3.0494	80.684	315	2.5991	76.856	315

O2	2.5388	129.89	0	2.4884	127.95	0	2.4677	127.45	0	2.4800	129.19	0
O2	2.5388	129.89	90	2.4884	127.95	90	2.4677	127.45	90	2.4800	129.19	90
O2	2.5388	129.89	180	2.5806	129.76	180	2.4677	127.45	180	2.4800	129.19	180
O2	2.5388	129.89	270	2.5806	129.76	270	2.4677	127.45	270	2.4800	129.19	270
O3	3.1929	37.60	0	3.1504	38.098	0	3.1948	38.245	0	3.2140	37.157	0
O3	3.1929	37.60	90	3.1504	38.098	90	3.1948	38.245	90	3.2140	37.157	90
O3	3.1929	37.60	180	3.2994	36.883	180	3.1948	38.245	180	3.2140	37.157	180
O3	3.1929	37.60	270	3.2994	36.883	270	3.1948	38.245	270	3.2140	37.157	270

Table S3. The ligand bond lengths (in [Å]) and the angular positions (in [°]) of O^{2-} ligands in the $[Ti\text{-}O_6]^{8-}$ cluster for the Gd^{3+} center in $PbTiO_3$ at different temperatures and structural phases obtained from the cif file.[21] RT – room temperature.

Temp.	10 K (tetragonal phase)			RT (tetragonal phase)			800 K (cubic phase)		
Ligand	R_{i0}	θ_i	φ_i	R_{i0}	θ_i	φ_i	R_{i0}	θ_i	φ_i
O1	2.3762	0	0	2.2515	0	0	1.985	0	0
O1	1.7628	180	0	1.8865	180	0	1.985	180	0
O2	1.9703	80.362	0	2.0026	76.753	0	1.985	90	0
O2	1.9703	80.362	90	2.0026	76.753	90	1.985	90	90
O2	1.9703	80.362	180	2.0026	76.753	180	1.985	90	180
O2	1.9703	80.362	270	2.0026	76.753	270	1.985	90	270

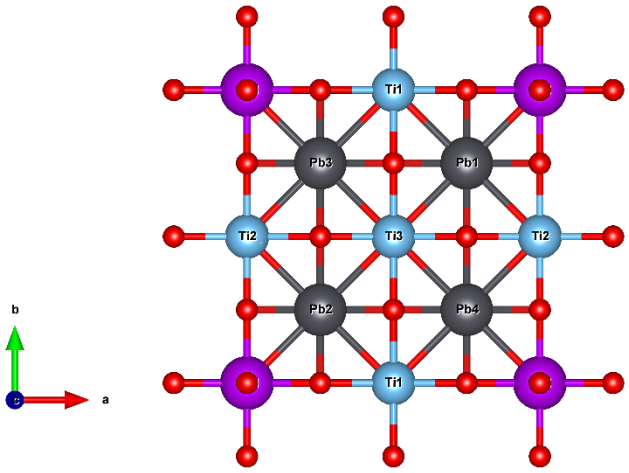

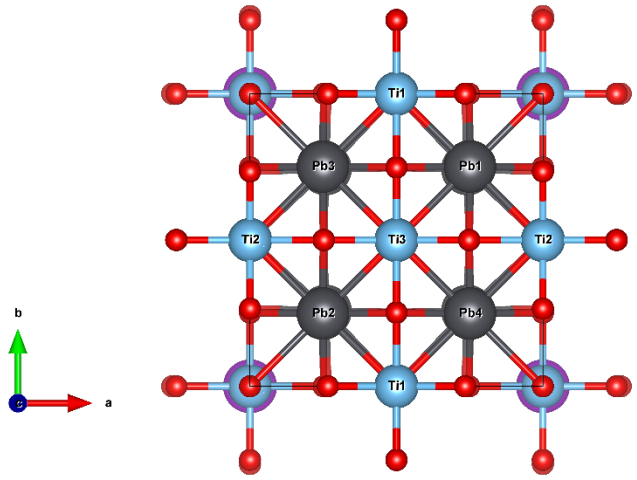

Fig. S1. Structure of $PbTi_{0.875}Gd_{0.125}O_3$ obtained using data in respective Tables: (a) non-relaxed structure (Table S1) and (b) optimized relaxed structure (Table S1).

Table S4. The ligand bond lengths (in [Å]) and the angular positions (in [°]) of O^{2-} ligands in the $[Pb\text{-}O_{12}]^{22-}$ cluster for the Gd^{3+} center in $PbTiO_3$ at different temperatures and structural phases obtained from the cif file. [21]

Temp.	10 K (tetragonal phase)			RT (tetragonal phase)			800 K (cubic phase)		
Ligand	R_{i0}	θ_i	φ_i	R_{i0}	θ_i	φ_i	R_{i0}	θ_i	φ_i
O1	2.7858	80.439	45	2.7738	83.653	45	2.807	90	45
O1	2.7858	80.439	135	2.7738	83.653	135	2.807	90	135
O1	2.7858	80.439	225	2.7738	83.653	225	2.807	90	225
O1	2.7858	80.439	315	2.7738	83.653	315	2.807	90	315
O2	2.5062	129.188	0	2.4511	127.318	0	2.807	135	0
O2	2.5062	129.188	90	2.4511	127.318	90	2.807	135	90
O2	2.5062	129.188	180	2.4511	127.318	180	2.807	135	180
O2	2.5062	129.188	270	2.4511	127.318	270	2.807	135	270
O3	3.2099	37.240	0	3.291	36.317	0	2.807	45	0
O3	3.2099	37.240	90	3.291	36.317	90	2.807	45	90
O3	3.2099	37.240	180	3.291	36.317	180	2.807	45	180
O3	3.2099	37.240	270	3.291	36.317	270	2.807	45	270

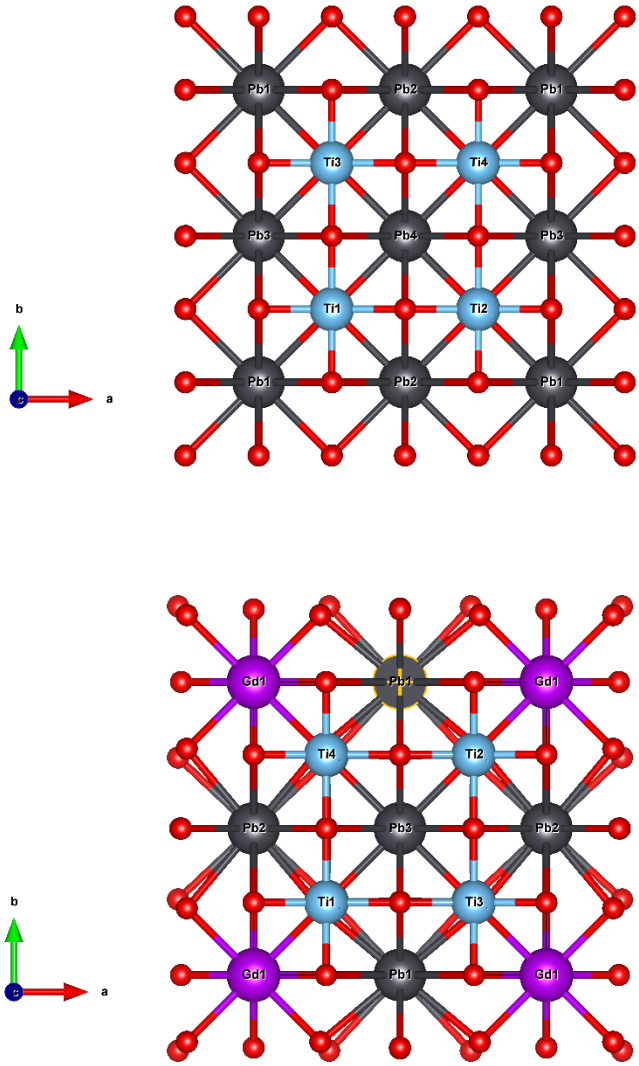

Fig. S2. Structure of $Pb_{0.875}Gd_{0.125}TiO_3$ obtained using data in respective Tables: (a) non-relaxed structure (Table S2) and (b) optimized relaxed structure (Table S2).

Table S5. The ligand bond lengths (in [Å]) and the angular positions (in [°]) of O^{2-} ligands for the Gd^{3+} center for the optimized relaxed structure with an O1-vacancy (O_{v1}): (a) for Ti-site in $PbTi_{0.875}Gd_{0.125}O_{3-\delta}$ and (b) for Pb-site in $Pb_{0.875}Gd_{0.125}TiO_{3-\delta}$.

(a)	Ti-site			(b) Pb-site			
Ligand	R_{i0}	θ_i	φ_i	Ligand	R_{i0}	θ_i	φ_i
O1	2.1158	180	0	O1	2.6576	76.745	47.53
O2	2.2014	76.611	0	O1	2.6953	76.934	223.4
O2	2.2014	76.611	90	O1	2.5609	76.920	315.0
O2	2.2014	76.611	180	O2	2.4090	128.46	1.911

O2	2.2014	76.611	270	O2	2.4672	125.96	92.42
				O2	2.4672	125.96	177.6
				O2	2.4091	128.46	268.1
				O3	3.3530	34.529	1.558
				O3	3.3598	36.844	91.91
				O3	3.3598	36.844	178.1
				O3	3.3530	34.529	268.4

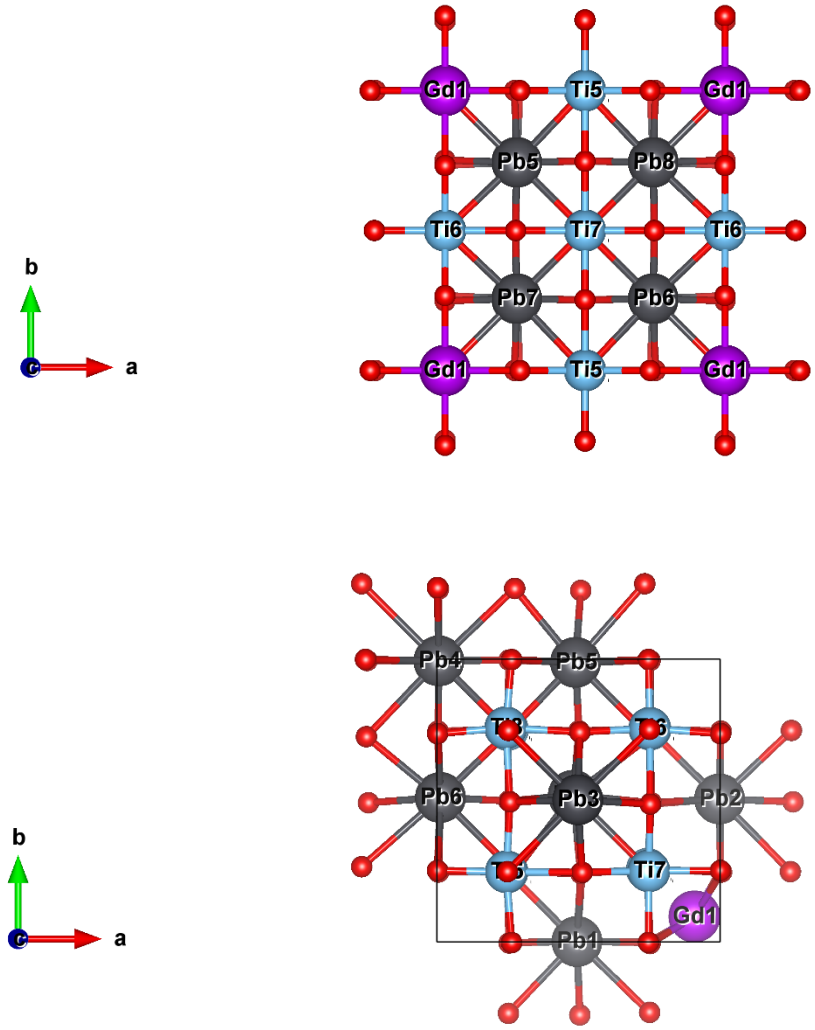

Fig. S3. Optimized relaxed structure of $Pb_{0.875}Gd_{0.125}TiO_{3-\delta}$ obtained for models assuming the presence of O-vacancy: (iii) Gd^{3+} at Ti-site (upper part) and (ii) Gd^{3+} at Pb-site (lower part).

[1] D.J. Newman, W. Urban, *Adv. Phys*, 1975, **24**, 793-844.

[2] M. Andrut, M. Wildner, C. Rudowicz, *Optical absorption spectroscopy in geosciences. Part II, Quantitative aspects of crystal fields, in A. Beran and E. Libowitzky (Eds) Spectroscopic Methods in Mineralogy - European Mineralogical Union Notes in Mineralogy* (Vol. 6 Budapest: Eötvös University Press Ch. 4) p 145, 2004.

[3] C. Rudowicz, P. Gnutek, M. Açikgöz, *Appl. Spectrosc. Rev*., 2019, **54** (8), 673-718.
[4] N. Ashcroft, N. Mermin, and N. Mermin, Solid State Physics, HRW international editions (Holt, Rinehart and Winston, 1976).
[5] C. Kittel, Introduction to Solid State Physics (Wiley, 1996).
[6] M. Yazdani-Kachoei, S. Rahimi, R. Ebrahimi-Jaberi, J. Nematollahi, and S. Jalali-Asadabadi, *Scientific Reports*, 2022 **12**, 663.
[7] M. Yazdani-Kachoei, S. Jalali-Asadabadi, *RSC Advances*, 2019 **9**, 36182.
[8] M. Shafiq, Iftikhar Ahmad, S. Jalali-Asadabadi, *RSC Advances*, 2015, **5**, 31496.
[9] M. Shafiq, Iftikhar Ahmad, and S. Jalali Asadabadi, *J. Appl. Phys*., 2014, **116**, 103905.
[10] M. Zarshenas, S. Jalali Asadabadi, *Thin Solid Film*, 2012, **520**, 2901-2908.
[11] A.D. Becke, *J. Chem. Phys*., 1993, **98**, 1372–1377.
[12] M. Yazdani-Kachoei, S. Jalali-Asadabadi, I. Ahmad, and K. Zarringhalam, *Scientific Reports*, 20016, **6**, 1-17.
[13] P. Blaha, K. Schwarz, G.K.H. Madsen, D. Kvasnicka, J. Luitz, *WIEN2k: An Augmented Plane Waves plus Local Orbitals Program for Calculating Crystal Properties*, Vienna University of Technology, Austria, (2001).
[14] P. Novák, J. Kuneš, L. Chaput, and W. E. Pickett, *physica status solidi (b)*, 2006, **243**, 559.
[15] L. Bjaalie, A. Verma, B. Himmetoglu, A. Janotti, S. Raghavan, V. Protasenko, E. H. Steenbergen, D. Jena, S. Stemmer, and C. G. Van de Walle*, Phys. Rev. B*, 2015, **92**, 085111.
[16] S. Gasiorowicz, Quantum Physics, 1974.
[17] M. Rafiee, S. Jalali Asadabadi, *Computational Materials Science*, 2009, **47**, 584.
[18] J. P. Desclaux, Comp. Phys. Commun., 1975, **9**, 31-45.
[19] Singh, David J., and Lars Nordstrom. Planewaves, Pseudopotentials, and the Linearized APW (LAPW) method. Springer Science & Business Media, 2006.
[20] E. Ghasemikhah, S. Jalali-Asadabadi, I. Ahmad, and M. Yazdani-Kachoei, *RSC Advances*, 2015, **5,** 37592.
[21] A.M. Glazer, S.A. Mabud, *Acta Crystallographica B*, 1978, **34**, 1065-1070.